



Proximity-induced amplification cascade for accurate and sensitive colorimetric detection of tumor-derived exosomes

Xiong Zhao^a, Ying Deng^b, Kaiyuan Liu^c, Jiating Xiao^c, Haohua Ren^c, Sha Ou^c, Beibei Kou^d, Shuai Wu^{e,*}, Zuquan Hu^{c,*}, Ying Peng^{c,*}

^a School of Medicine And Health Management, Guizhou Medical University, Guiyang 550025, China

^b State Key Laboratory of Analytical Chemistry for Life Science, School of Life Sciences, Nanjing University, Nanjing 210023, China

^c Immune Cells and Antibody Engineering Research Center in University of Guizhou Province, Key Laboratory of Biology and Medical Engineering, School of Biology and Engineering (School of Modern Industry for Health and Medicine), Guizhou Medical University, Guiyang 550025, China

^d State Key Laboratory of High-efficiency Utilization of Coal and Green Chemical Engineering, Ningxia University, Yinchuan, Ningxia 750021, China

^e Clinical Research Center, The First Affiliated Hospital with Nanjing Medical University, Nanjing, Jiangsu 210029, China

ARTICLE INFO

Keywords:

Proximity-induced amplification cascade
DNA-Pt@AuNPs signal probes
Multivalent capture interface
Clinical cancer diagnosis

ABSTRACT

Tumor-derived exosomes have garnered immense interest as potential molecular markers for noninvasive diagnosis, treatment, and prognostic evaluation of cancer. Herein, we have reported a proximity-induced amplification cascade for achieving accurate and sensitive colorimetric detection of tumor-derived exosomes. Specifically, the proximity hybridization effect triggered by the binding of two aptamers to the adjacent proteins on the surface of the target exosomes will lead to the release of the trigger strand, initiating a cascade of subsequent three-way catalytic hairpin assembly and rolling circle amplification reactions. Consequently, a substantial amount of single-strand DNA will be generated, which can bind to numerous DNA-Pt@AuNPs signal probes and be efficiently captured by the multivalent capture interface, leading to dramatically intensified colorimetric signals for sensitive detection of tumor-derived exosomes. Benefiting from the synergy of multiple signal amplification strategies, a detection limit as low as 194 particles μL^{-1} has been achieved. In addition, the dual-molecular recognition enabled by proximity effect endows the sensing platform with excellent selectivity to distinguish target exosomes from other interfering exosomes, cell fragments and proteins. Notably, the proposed sensing platform can be successfully applied to the detection of targets in serum samples and can distinguish between MUC1/EpCAM-positive breast cancer patients from healthy individuals, highlighting its promising potential in clinical cancer diagnosis.

1. Introduction

Cancer is one of the leading causes of human death and has become a major global public health issue [1,2]. Despite the unprecedented progress in cancer treatment over the past decade, most metastatic tumors remain incurable. Therefore, precise early diagnosis of cancer continues to be one of the most crucial strategies to overcome the threat of cancer [3–5]. In recent years, liquid biopsy biomarkers have emerged as significant “molecular signatures” for diagnosis of cancer [6,7]. In particular, tumor-derived exosomes, as novel biomarkers for liquid biopsy, have garnered considerable attention in the diagnosis and treatment of cancer [8,9]. Exosomes are a type of phospholipid bilayer vesicles with a nanometer-sized diameter ranging from 30 nm to

150 nm. They are secreted by their parent cells and can be found in various body fluids [10]. Studies have demonstrated that tumor-derived exosomes contain abundant bioinformation of primary tumors, such as specific DNA fragments, microRNAs and proteins, and their quantity in body fluids is closely associated with cancer progression [10–12]. Therefore, the detection and analysis of tumor-derived exosomes hold the potential to emerge as a pivotal research frontier of cancer diagnostics.

Traditional methods for quantifying exosomes include tunable resistive pulse sensing [13], flow cytometry [14,15], as well as nanoparticle tracking analysis [16]. However, high operational costs and limited selectivity hinder their application in assays of tumor-derived exosomes. In recent years, innovative detection strategies rooted in

* Corresponding authors.

E-mail addresses: shwu@njmu.edu.cn (S. Wu), huzuquan@gmc.edu.cn (Z. Hu), peng_ying@gmc.edu.cn (Y. Peng).

<https://doi.org/10.1016/j.snb.2025.137832>

Received 2 December 2024; Received in revised form 28 March 2025; Accepted 18 April 2025

Available online 21 April 2025

0925-4005/© 2025 Elsevier B.V. All rights are reserved, including those for text and data mining, AI training, and similar technologies.

the recognition of surface proteins of exosomes have emerged, including colorimetry [17], electrochemistry [18–20], and microfluidic [21] strategies, aiming to enhance exosome detection performance. Among these, colorimetric technology has garnered significant attention due to its ability to facilitate convenient, rapid, and efficient visual analysis without specialized equipment. Notably, following the advent of nanozymes, the merits of colorimetric biosensors in terms of stability, ease of operation, and cost-effectiveness have been further underscored [22]. An illustrative case of functional nanozyme design is platinum-coated gold nanoparticles (Pt@AuNPs), which integrate the peroxidase-like catalysis of platinum and the biocompatibility [23]. The unique core-shell architecture ensures robust catalytic stability and supports high-density DNA conjugation, which is indispensable for signal amplification in low-abundance exosome detection. This core-shell design simultaneously addresses catalytic durability and functional versatility. However, conventional nanozyme-based platforms relying on single-target recognition fail to address the inherent heterogeneity of exosomes and interference from biomolecular contaminants such as cell fragments or free proteins [24,25]. Consequently, there is a pressing demand to integrate dual-molecular recognition strategies into colorimetric analysis systems, thereby significantly enhancing the accuracy of exosome identification.

The proximity effect provides new possibilities for the dual-molecular recognition residing on the membrane structures. This phenomenon inherently involves the simultaneous binding of two affinity probes (or proximity probes—pairs of ligands engineered to bind spatially adjacent epitopes on a target structure, such as proteins or membrane-bound vesicles) to trigger localized hybridization or assembly events. [26,27]. This orchestrated binding can facilitate binding-induced strand displacement reactions or assembly between affinity probes, ultimately leading to the generation of detectable signals. Notably, amidst the complexities of dual-target recognition for exosome analysis, one of the paramount challenges lies in the attenuation of signal response [28]. Essentially, the proximity effect enhances the specificity in exosome recognition through identifying dual-target proteins on membrane structures. However, the simultaneous recognition of dual sites paradoxically leads to signal attenuation, inevitably compromising sensitivity. Therefore, enhancing sensitivity is crucial for detecting ultra-low abundance exosomes.

In response, we have proposed a proximity-induced dual-target recognition strategy coupled with cascade amplification, aiming to achieve both high specificity and sensitivity. In our design, the proximity hybridization effect initiates a three-way catalytic hairpin assembly (3W-CHA)—a dynamic DNA circuit where three metastable hairpin probes (HP1–3) undergo sequential strand displacement reactions to form a Y-shaped DNA structure with the recycling of trigger strand. This process, coupled with rolling circle amplification (RCA) [29, 30], generates abundant long single-stranded DNA products. Subsequently, these DNA strands are hybridized with DNA-functionalized platinum-coated gold nanoparticles (DNA-Pt@AuNPs) nanozyme and simultaneously captured by the multivalent capture interface. Upon incubation with H_2O_2 and TMB, remarkably intensified colorimetric changes will be observed, facilitating target quantification. Our proposed colorimetric biosensor showcases several notable advancements. Firstly, the proximity effect significantly improves the specificity of exosome recognition through simultaneous binding of two biomarkers (MUC1 and EpCAM). This dual-target design effectively mitigates interference from non-target entities (e.g., cell fragments, free proteins, or single-positive exosomes) and suppresses false-positive signals, highlighting the promise of non-invasive liquid biopsy using serum exosomes for accurately predicting cancer origin. Secondly, by integrating multiple amplification strategies of 3W-CHA, RCA reaction, nanozyme catalysis, and multivalent capture mechanisms, significantly enhanced colorimetric signals will be generated, which is beneficial for quantitative analysis of low abundance exosomes. Thirdly, our colorimetric biosensor demonstrates potential as a candidate tool for

point-of-care testing (POCT), owing to its extremely convenient measurements (e.g., equipment-free naked-eye assessment or basic spectrophotometric quantification, and operator-friendly procedures without repetitive washing), and cost-effectiveness, which may support clinical cancer diagnosis in settings with limited resources.

2. Experimental section

Chemicals and materials, pretreatment of clinical sample, western blot assay and capture efficiency evaluation detailed in [Supplementary information](#).

2.1. Preparation of Au nanoparticles (AuNPs)

AuNPs were prepared in accordance with a previously reported method, with slight modifications incorporated [23]. Briefly, 40 mL of 2.2 mM sodium citrate solution was added to a clean conical flask and vigorously stirred for 5 min within a water bath maintained at 100 °C. Promptly thereafter, 267 μL of 25 mM HAuCl_4 was swiftly added to initiate the reaction, which was allowed to proceed until the emergence of a wine-red hue in the solution, typically observed within approximately 10 min. Subsequently, the reaction temperature was adjusted to 90 °C and maintained for 10 min. Using a syringe pump (Longer Precision Pump Co., Ltd, China) to ensure precise flow rate control, 267 μL of 60 mM sodium citrate solution was added, followed by the addition of 267 μL of 25 mM HAuCl_4 solution after 2 min. Stirring was continued for another 30 min to ensure the formation of AuNPs. Upon completion and subsequent cooling, the prepared AuNPs were carefully stored in a dark environment at 4 °C for future use.

2.2. Preparation of platinum-coated AuNPs (Pt@AuNPs)

Pt@AuNPs were prepared based on prior research with minor modifications [23]. Initially, 16 mL of AuNPs solution was warmed in a 90 °C water bath for 5 min. To achieve precise and gradual reagent delivery, 694 μL of 1.0 mM Na_2PtCl_6 solution was introduced via a syringe pump at a controlled flow rate of 20 $\mu\text{L min}^{-1}$, immediately followed by the addition of 8 mL of 4.0 mM L-ascorbic acid at a rate of 40 $\mu\text{L min}^{-1}$ using the same pump system, ensuring a gradual yet efficient mixing of the reactants. Following a 30-min reaction period, the resulting Pt@AuNPs were cooled to 25 °C and then preserved in a dark environment for future applications.

2.3. Preparation of DNA-Pt@AuNPs

The freezing approach was adopted to prepare DNA-Pt@AuNPs. Freezing enhances DNA loading density on Pt@AuNPs through ice crystal exclusion effect, which concentrate nanoparticles, DNA, and ions into localized micro-pockets to accelerate thiolated DNA conjugation via Pt-S/Au-S bonds. This process stabilizes thiol-metal interactions and minimizes nonspecific binding [31,32]. Specifically, 10 μL of 100 μM HS-DNA was mixed with 200 μL of the prepared Pt@AuNPs. This mixture was then subjected to cryopreservation at -20 °C for 3 hours, allowing for efficient interaction between the DNA and nanoparticles. Following natural thawing at room temperature, the mixture underwent centrifugation at 11,500 rpm for 10 min, effectively separating and discarding the unbound HS-DNA in the supernatant. Subsequently, the precipitate, enriched with DNA-Pt@AuNPs, was washed three times with PBS buffer to eliminate impurities. Finally, the purified DNA-Pt@AuNPs product was redispersed in PBS and stored under refrigerated conditions (4 °C) in a dark environment, ensuring its stability and readiness for subsequent applications.

2.4. Preparation of the sensing probes

Prior to the experiment, the oligonucleotides AP1, HP1, HP2, HP3

along with the blend of AP2 and TS, underwent an annealing process in Tris-HCl buffer; which involved maintaining the mixture at 95 °C for 10 min, followed by a gradual cooling to room temperature.

Similarly, to prepare circular DNA1 and circular DNA2 (denoted as cDNA1 and cDNA2), the combinations of L1 (1.2 μM) with PS1 (1 μM), and L2 (1.2 μM) with PS2 (1 μM) were annealed using the same annealing protocol described above. To seal the nicks in the L1/PS1 and L2/PS2 duplexes, T4 DNA ligase (30 U) was incubated with the respective duplexes overnight. Following this, the T4 DNA ligase was inactivated through high-temperature treatment (70 °C for 10 min). Subsequently, exonucleases I and exonuclease III (each at 100 U) were introduced and incubated for 60 min to degrade linear DNA remnants. Once the digestion was complete, both exonucleases were likewise inactivated in a high-temperature environment (80 °C for 10 min). Ultimately, the prepared cDNA1 and cDNA2 were stored at 4 °C for subsequent experimentation and future utilization.

2.5. Cell culture and exosomes extraction

All pertinent cell lines were propagated in DMEM medium that was enriched with penicillin-streptomycin (1 %) and exosome-depleted FBS (10 %), within a humid environment that maintained a stable concentration of 5 % CO₂ at a constant temperature of 37 °C. After 48 hours of cell culture, the cell supernatant was collected. Initially, to eliminate intact cells and larger biomolecules, the culture medium underwent a two-step centrifugation process: firstly at 5000 g for 10 min, followed by 10,000 g for an additional 30 min. Subsequently, the obtained supernatant underwent filtration through a high-precision membrane with a pore diameter of 0.22 μm. Thereafter, the filtered supernatant underwent ultra-centrifugation at 120,000 g for 70 min, yielding exosome pellets. These pellets were then carefully washed with sterile PBS buffer to ensure purity and stored at −80 °C for future applications and analysis.

2.6. Construction of the multivalent capture interface

Firstly, the biotinylated strand (BS) and the streptavidin-coated high-capacity plates were incubated together for 2 h at 37 °C. Subsequently, the RCA reaction was initiated by incubating the reaction mixture, which comprised 1 × polymerase buffer, dNTP (1 mM), phi29 DNA polymerase (10 U) and cDNA1 (1 μM) for 40 min. Lastly, the plates underwent a thorough rinsing process three times with Tris-HCl solution to remove any residual polymerase enzymes and excess nucleic acid sequences.

2.7. Detection of exosomes

Initially, exosomes of diverse concentrations were subjected to a 2 h reaction within a mixture consisting of AP1, AP2/TS, HP1, HP2, HP3, dNTPs (1 mM), phi29 DNA polymerase (10 U), and cDNA2 (1 μM). Afterward, the resulting reaction solution was incubated with DNA-Pt@AuNPs (25 μL) and the multivalent capture interface for 30 min to ensure effective binding among the RCA products, DNA-Pt@AuNPs, and the capture interface. Upon rinsing with PBS to remove unbound components, the capture interface was further incubated with TMB-H₂O₂ (50 μL) in the dark for 30 min to initiate the peroxidation reaction. This reaction facilitated the generation of distinct, visually discernible colors, allowing for qualitative analysis by the naked eye. Ultimately, the peroxidation reaction was terminated by the addition of H₂SO₄ (1 M, 100 μL), enabling the subsequent measurement of absorbance using UV-spectroscopy (UV-1800, Shimadzu, Japan) for precise quantitative analysis.

2.8. Flow cytometry

In the initial step, 30 μL of 100 μM biotinylated CD63 aptamer was

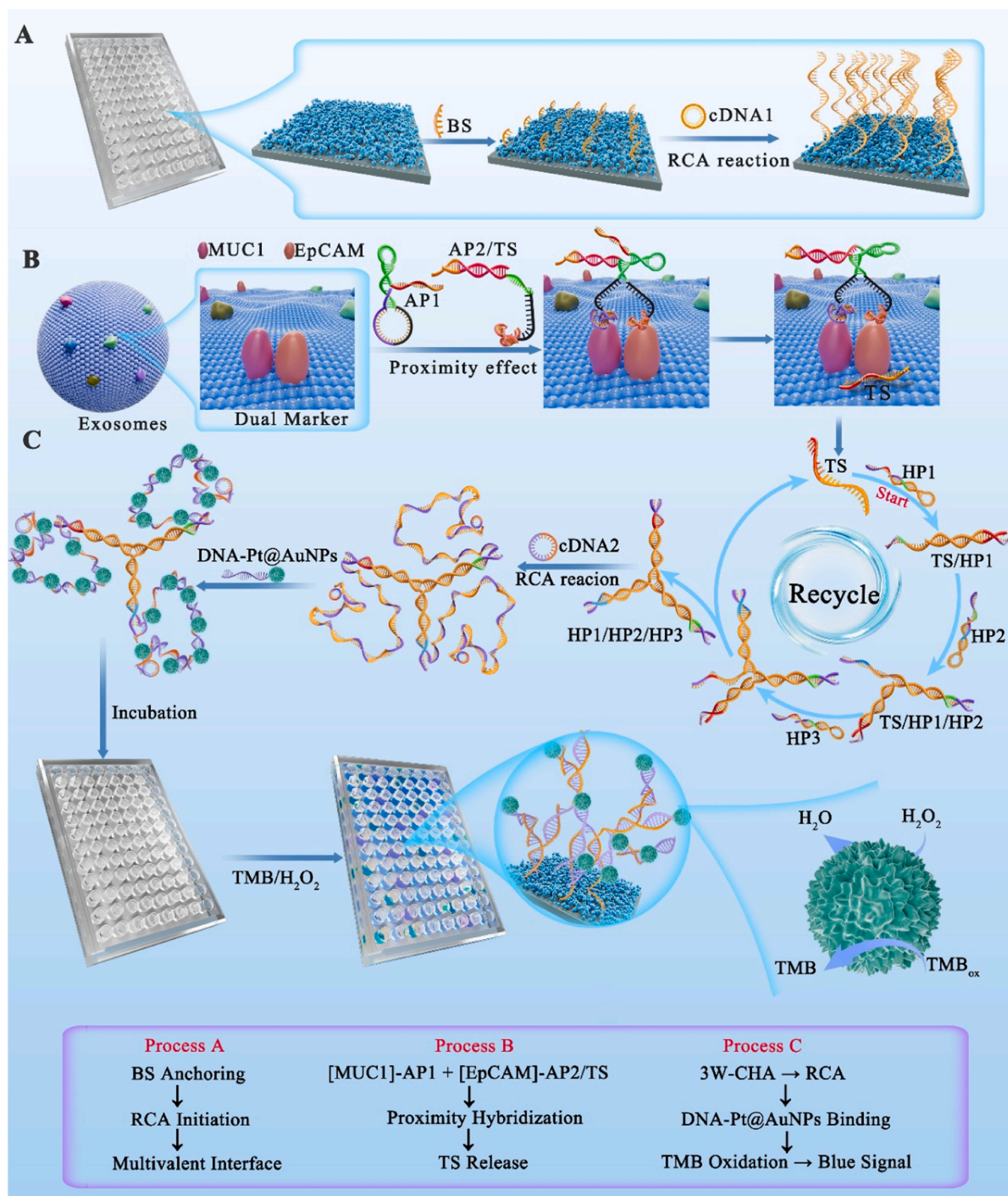
added to 100 μL of streptavidin-coated magnetic beads, followed by a 2 h incubation to allow for binding. Subsequently, the unbound biotinylated CD63 aptamer was removed using magnetic separation. Finally, the treated magnetic beads were stored in 1 mL of PBS for further analysis.

Next, 2 μL of aptamer-modified magnetic beads were incubated with exosomes at 37 °C for 1 h to facilitate binding. Following rinsing with PBS to remove unbound components, 1 μM of nucleic acid probes were added, and incubation was continued for 1 h to allow for probe hybridization. The sample was then washed three times with PBS to remove any unbound probes and resuspended in PBS buffer. Finally, the sample was analyzed using a flow cytometer.

3. Results and discussion

3.1. Working principle

The principle of the proposed colorimetric biosensing strategy is illustrated in [Scheme 1](#). Process A depicts the fabrication process of the capture interface via streptavidin-biotin interaction. Firstly, the biotinylated BS sequence is anchored onto a streptavidin-coated microplate. Subsequently, cDNA1, phi29 polymerase, and dNTPs are added, enabling the in-situ generation of long ssDNA containing numerous repeated capture domains through RCA reaction, thereby forming a robust and multivalent capture interface. Process B describes the dual-molecular recognition process of exosomes. Initially, a pair of proximity probes (AP1 and AP2/TS) is designed with multi-functional domains, comprising aptamer domains for molecular recognition (purple sequence in AP1 and orange sequence in AP2), spacer domains to mitigate spatial hindrance (black sequence), complementary domains (green sequence) for proximity hybridization, and strand displacement domains (red sequence) for the release of TS. The complementary domain in AP1 is locked in the stem of the hairpin structure, therefore, inhibiting hybridization between AP1 and AP2 in the absence of the target. Upon simultaneous binding of AP1 and AP2/TS to EpCAM and MUC1, respectively, which are abundantly expressed on the surface of MCF-7-derived exosomes, AP1 initially exposes its complementary domain. Subsequently, due to the proximity effect, AP1 and AP2 undergo stable hybridization triggering a strand displacement reaction that releases TS, ultimately initiating a cascade of downstream amplification reactions. Process C represents the downstream amplification reaction process, which aims at amplifying signals emanating from exosome recognition. This process begins with three partially complementary hairpin structures (HP1, HP2 and HP3), which are rationally designed in metastable states. The two fragmented segments (purple sequence) of the complete RCA trigger sequence are inserted into the 3' and 5' termini of these hairpins, respectively. In the absence of TS, the hybridization among the hairpins is severely hindered by the kinetic trap, effectively stalling the amplification cascade. However, upon the liberation of TS by the dual-molecular recognition on the surface of exosomes, downstream strand displacement reaction is triggered. TS firstly binds to the toehold domain (red sequence) of HP1, initiating the unraveling of the stem domain of HP1. The newly exposed toehold domain (green sequence) then promptly triggers the second strand displacement reaction, unfolding HP2. This sequential process repeats, with the exposed domain on HP2 initiating the third strand displacement reaction to unfold HP3, ultimately culminating in the formation of a Y-shaped structure comprising HP1, HP2, and HP3, along with the recycling of TS. This Y-shaped configuration brings the two fragmented RCA trigger segments into close proximity, reforming the complete RCA trigger sequence at the termini of each arm. Consequently, upon the addition of dNTPs, phi29 DNA polymerase, and cDNA2, the RCA reaction is initiated, yielding lengthy DNA products rich in numerous repeated units, each featuring two distinct functional domains (purple and yellow sequences). The purple domain, which is complementary to the DNA sequence modified on Pt@AuNPs, facilitates the attachment of



Scheme 1. Schematic illustration of the proximity-induced amplification cascade for exosomes detection: (A) Fabrication of the multivalent capture interface via streptavidin-biotin binding and RCA-driven ssDNA generation. (B) Dual-target recognition of exosomes by aptamers AP1 and AP2, triggering proximity hybridization and TS release. (C) TS initiates 3W-CHA (HP1/HP2/HP3) to form Y-shaped DNA, which triggers RCA for DNA-Pt@AuNPs assembly, enabling TMB oxidation catalysis for detection.

Pt@AuNPs to the RCA products through DNA hybridization. Simultaneously, the orange domain, through complementary hybridization with the multivalent capture probes on the capture interface, effectively pulls RCA products adorned with Pt@AuNPs toward this interface. Consequently, powered by the catalytic prowess of Pt@AuNPs, the H_2O_2 -mediated oxidation of TMB proceeds efficiently on the capture interface, yielding an obvious and pronounced intensified blue output signal that serves as a reliable indicator for the quantitative analysis of target exosomes.

3.2. Characterizations of Pt@AuNPs and DNA-Pt@AuNPs

To validate the prepared nanoparticles, the morphology of Pt@AuNPs was initially investigated using Transmission Electron Microscopy (TEM). As clearly depicted in Fig. 1 (A–C), uniformly spherical nanoparticles display excellent dispersibility. The size of these particles is consistent, with an average diameter of approximately 15.2 nm (Fig. 1F), which aligns with literature reports [23]. Additionally, an in-depth energy dispersive X-ray (EDX) mapping of individual particles was performed. As shown in Fig. 1D, the two elements Au (red) and Pt

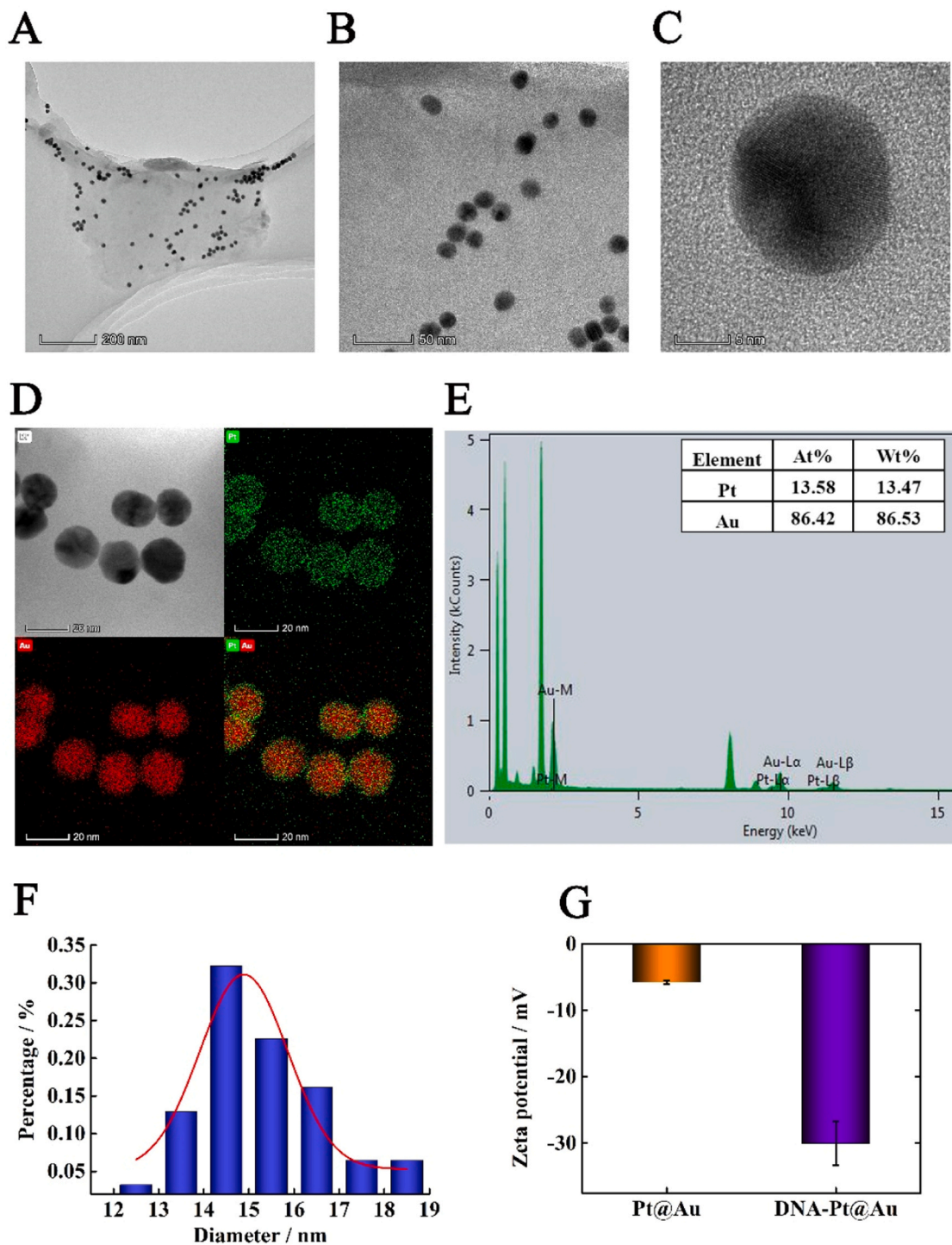


Fig. 1. (A–C) TEM image of the Pt@AuNPs. (D) EDX mapping image of Pt@AuNPs (green = Pt, red = Au). (E) EDS spectrum of Pt@AuNPs. (F) Particle size distribution of Pt@AuNPs. (G) Zeta potential of Pt@AuNPs and DNA-Pt@AuNPs.

(green) are densely distributed within the particles, with Au residing at the core of the nanoparticles; while Pt coats the surface, conclusively demonstrating the successful formation of a core-shell structure in Pt@AuNPs. Furthermore, as shown in Fig. 1E, the as-synthesized Pt@AuNPs are composed of Au and Pt elements, with the atomic fraction of Au and Pt being approximately 86.42 % and 13.58 %, respectively. Subsequently, we assessed the catalytic performance of the synthesized Pt@AuNPs. As depicted in Fig. S1, upon the incremental incorporation of Pt@AuNPs, a discernible trend emerges: the UV-Vis absorption intensity at 450 nm steadily increases, concomitantly enhancing the bluish hue of the substrate solution. In stark contrast, the AuNPs without platinum plating exhibit a significantly diminished absorption at 450 nm, thereby demonstrating the superiority of our prepared Pt@AuNPs as ideal colorimetric detection probes. The enzyme reaction kinetics analysis of the synthesized Pt@AuNPs further provides compelling evidence for their formidable catalytic capability, as evidenced by the results presented in Fig. S2. Dynamic light scattering confirmed the loading of DNA on the surface of Pt@AuNPs. As shown in Fig. S3, the hydrodynamic diameter of Pt@AuNPs increases from 46.6 nm to 84.1 nm after loading DNA. Moreover, the modification of DNA on Pt@AuNPs was conclusively verified through zeta potential measurements. As illustrated in Fig. 1G, the zeta potential value corresponding to Pt@AuNPs alone is approximately -5.75 mV. However, after the introduction of DNA, the zeta potential decreases to approximately -30 mV, attributable to the negatively charged phosphate backbone of DNA, demonstrating the successful modification of DNA on Pt@AuNPs. As shown in Fig. S4, DNA loading directly correlates with colorimetric signal intensity until saturation at $10 \mu\text{L}$ HS-DNA (~ 366 DNA strands per particle), beyond which steric hindrance limits amplification efficiency. This highlights the critical balance between maximizing DNA density and maintaining nanoparticle functionality. Additionally, the catalytic stability of DNA-Pt@AuNPs was rigorously evaluated under varying conditions. As shown in Fig. S5A, DNA-Pt@AuNPs retain > 90 % of their initial catalytic activity after 30 days of storage at 4°C , demonstrating robust long-term stability. The stability of DNA-Pt@AuNPs was further validated through repeated freeze-thaw cycles (up to 5 cycles), with no significant loss in catalytic activity (Fig. S5B). These results underscore the reliability of Pt@AuNPs as durable and versatile signal probes.

3.3. Feasibility exploration

After successful extraction and characterization of the exosomes (Fig. S6), the feasibility of the dual-molecular recognition mechanism was verified using flow cytometry. As illustrated in Fig. 2A, in the dual-target recognition group (Group c), simultaneous binding of AP1 (EpCAM) and AP2-FAM/TS-BHQ (MUC1) triggers proximity hybridization, displacing TS-BHQ and separating the FAM fluorophore from the quencher. This results in an approximately 3-fold fluorescence enhancement compared to single-target groups (Groups a and b), where fluorescence remained quenched due to intact FAM-BHQ proximity. In Group a, only the recognition probe targeting MUC1 is used, whereas in Group b, only the recognition probe targeting EpCAM is employed. The result indicates that the release of TS-BHQ is contingent upon the simultaneous binding of both recognition probes to the surface of the target exosomes. Meanwhile, the efficiency of strand displacement reactions induced by the proximity effect and free diffusion was also evaluated. As depicted in Fig. S7, for the same strand displacement process, the signal measured in the reaction system is significantly enhanced when the proximity effect is present. This demonstrates that the proximity effect, beyond enabling the system to recognize dual molecules, is a crucial determinant in boosting its sensitivity. Moreover, the UV-Vis spectra of the captured interface, when incubated with different reaction solutions, was monitored for verification of the feasibility of the proposed colorimetric sensing platform. As shown in Fig. 2B, a weak UV-Vis absorption peak is observed at 450 nm after the

capture interface is incubated with TMB- H_2O_2 and DNA-Pt@AuNPs, possibly due to the weak non-specific adsorption of DNA-Pt@AuNPs by the capture interface. The addition of AP1, AP2/TS, HP1, HP2, HP3, phi29 and dNTP results in slightly enhanced UV-Vis absorption peak at 450 nm, which may be attributed to the weak non-specific assembly between DNA probes. In stark contrast, further introduction of the target leads to a sharp increase in signal response, suggesting successful initiation of 3W-CHA/RCA to form long DNA products, and the subsequent binding of the DNA products and Pt@AuNPs to the capture interface. Finally, we have also fabricated a monovalent capture interface and compared it with our designed multivalent capture interface. As shown in Fig. 2C, the signal response from the multivalent capture interface exhibits significant enhancement with same experimental conditions, clearly highlighting the advantage of our constructed multivalent capture interface in enhancing sensitivity. To further evaluate the performance of the capture interfaces, we quantified exosome capture efficiency by comparing total protein content of lysed exosomes before and after binding (Fig. S9). The multivalent capture interface achieves a capture efficiency of 78.5 %, significantly surpassing the monovalent interface (46.7 %), underscoring its superior avidity and practical utility in exosome enrichment.

3.4. Sensitivity exploration

To assess the analytical performance of the devised colorimetric biosensor, a series of concentration targets were incorporated into the testing phase, following the optimization of key experimental conditions, including the volume of DNA-Pt@Au, the concentration of BS, the RCA reaction time during the construction of the capture interface, and the reaction time (Fig. S10). Fig. 3A illustrates that as the target concentration increases from 7.20×10^2 to 1.44×10^6 particles μL^{-1} , the UV-Vis absorption intensity monitored at 450 nm exhibits a commensurate increase. This trend is in line with our predictions based on the mechanism of the system, as an elevated concentration of exosomes releases a profusion of RCA triggering sequences, prompting the generation of abundant RCA products, which subsequently bind with a large quantity of DNA-Pt@AuNPs to facilitate the peroxidation reaction. As evidently illustrated in Fig. 3B, a linear correlation is observed between the absorbance intensity at 450 nm and the logarithm of target abundance from 7.20×10^2 to 1.44×10^6 particles μL^{-1} . The regression equation is fitted as $A = 0.4080 \log c - 1.0478$ (where A represents the absorbance intensity at 450 nm, and c signifies the concentration of the target), with a low limit of detection (LOD) of 194 particles μL^{-1} , which is calculated according to the 3σ rule. The formula applied for this calculation is $\text{LOD} = 3\sigma/k$. Here, σ denotes the standard deviation of the blank group, while k represents the slope of the calibration curve within the lower concentration ranges. As depicted in Fig. 3C, the color intensity of the reaction solution, as observed by the naked eye, steadily intensifies with the increase of target concentration. This visual progression is consistent with the quantitative findings presented in Fig. 3A and 3B. Even targets with concentrations as low as 1.44×10^3 particles μL^{-1} can be distinguished by the naked eye when compared to the background color, further verifying the sensitivity of the constructed biosensor.

3.5. Investigations of anti-interference capability

Four different exosomes—specifically, MCF-7 cell-derived exosomes (MUC1-positive, EpCAM-positive), MCF-10A cell-derived exosomes (MUC1-negative, EpCAM-negative), HepG2 cell-derived exosomes (MUC1-negative, EpCAM-positive), and Hela cell-derived exosomes (MUC1-positive, EpCAM-negative)—were employed for selective evaluation. The selective evaluation was carried out by subjecting each type of exosome to the same detection procedure described in Section 2.7. Briefly, each type of exosome (1.44×10^5 particles μL^{-1}) was individually incubated with the sensing probes for the amplification cascade,

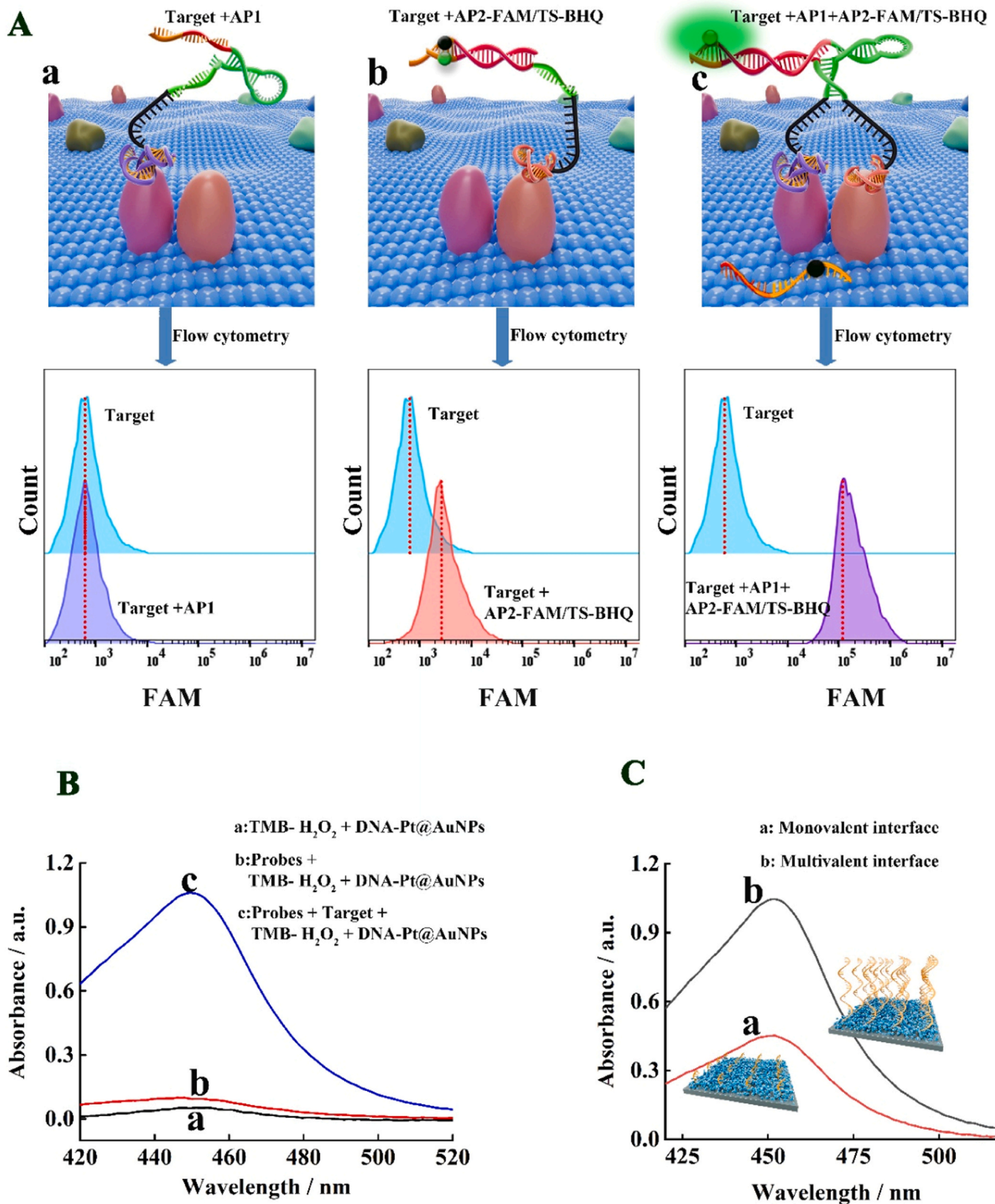


Fig. 2. (A) Flow cytometry results obtained using different recognition probes : (a) MUC1-only recognition, (b) EpCAM-only recognition, (c) simultaneous recognition of MUC1 and EpCAM. (B) UV-Vis absorption spectra of the multivalent capture interface upon incubation with varying reaction solutions: (a) TMB- H_2O_2 and DNA-Pt@AuNPs, (b) AP1, AP2/TS, HP1, HP2, HP3, cDNA2, phi29, dNTP, DNA-Pt@AuNPs and TMB- H_2O_2 , (c) target exosomes, AP1, AP2/TS, HP1, HP2, HP3, cDNA2, phi29, dNTP, DNA-Pt@AuNPs and TMB- H_2O_2 . (C) The UV-Vis absorption spectra recorded on different capture interface: (a) the monovalent capture interface, (b) the multivalent capture interface.

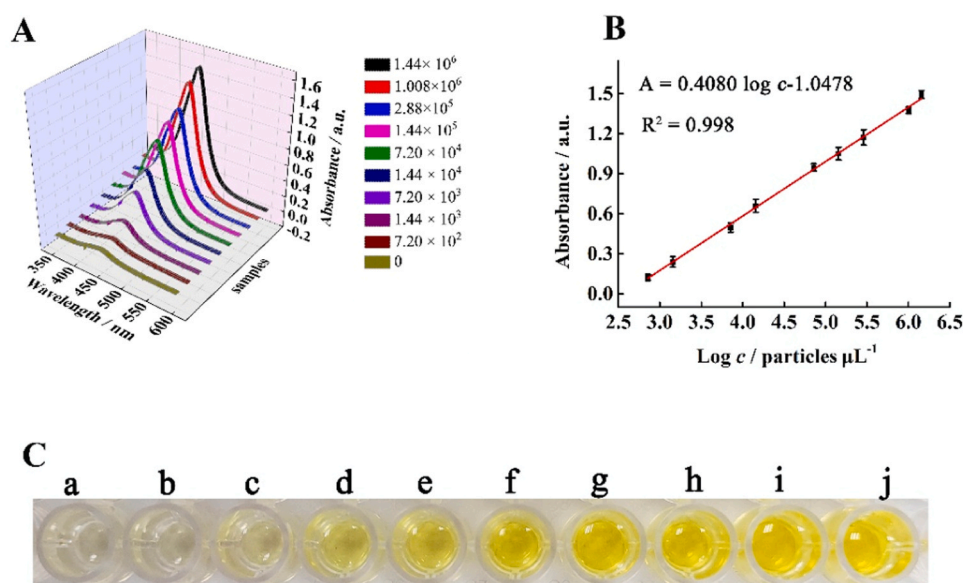


Fig. 3. (A) UV-Vis spectra of the developed colorimetric biosensor in the presence of different concentrations of targets (0 , 7.20×10^2 , 1.44×10^3 , 7.20×10^3 , 1.44×10^4 , 7.20×10^4 , 1.44×10^5 , 2.88×10^5 , 1.008×10^6 , 1.44×10^6 particles μL^{-1}). (B) Dependence of UV-Vis absorption intensity on the logarithm of target exosomes concentrations. (C) The photographs of reaction solutions incubated with different concentrations of targets (a-j): 0 , 7.20×10^2 , 1.44×10^3 , 7.20×10^3 , 1.44×10^4 , 7.20×10^4 , 1.44×10^5 , 2.88×10^5 , 1.008×10^6 , 1.44×10^6 particles μL^{-1}). Error bars: SD, $n = 3$.

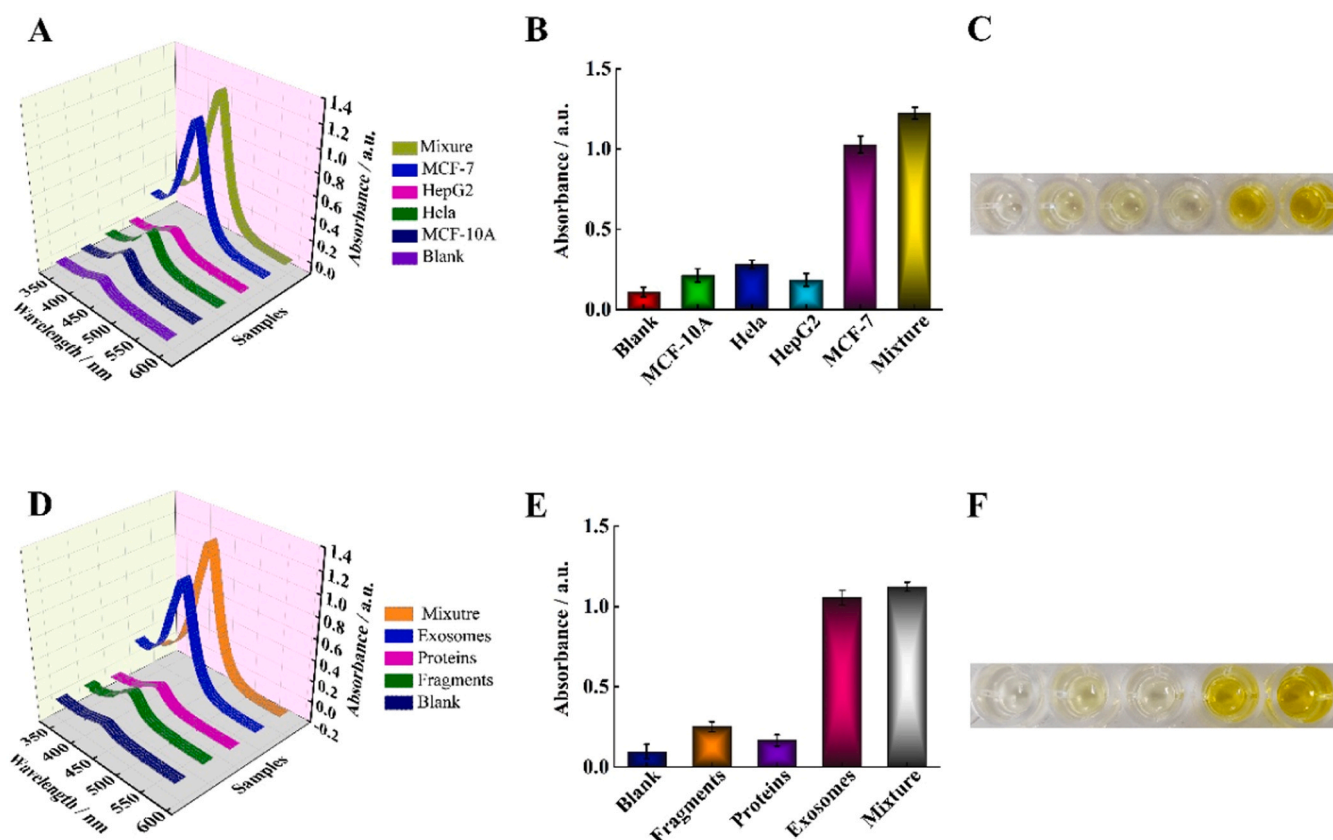


Fig. 4. (A) UV-Vis absorption spectra of the biosensor in the presence of exosomes derived from different cell lines. (B) Statistical results of the mean UV-Vis absorption peak intensities at 450 nm derived from triplicate measurements of the experiments shown in (A). (C) Photographs of the reaction solutions corresponding to the experiments shown in (A). (D) UV-Vis absorption spectra in the presence of interfering substances. (E) Statistical results of the mean UV-Vis absorption peak intensities at 450 nm derived from triplicate measurements of the experiments shown in (D). (F) Photographs of the reaction solutions corresponding to the experiments shown in (D). Error bars: SD, $n = 3$.

followed by the colorimetric signal measurement. Additionally, a mixture containing MCF-7-derived exosomes (target) and interfering exosomes (MCF-10A, HepG2, and Hela-derived exosomes at a 1:1:1 ratio) was tested to mimic complex biological samples. The UV-Vis absorption spectra and colorimetric responses were recorded under identical experimental conditions. As clearly demonstrated in Fig. 4A and 4B, the UV-Vis absorption peak of MCF-7 cell-derived exosomes exhibits a remarkable enhancement (signal-to-noise ratio = 9.22) compared to those derived from MCF-10A, Hela, and HepG2 cells, whose signals are indistinguishable from background levels (signal-to-noise ratio < 1.3). When a mixture of MCF-10A-derived, Hela-derived, and HepG2-derived exosomes is added to the target MCF-7-derived exosomes, the signal response only weakly enhances (signal-to-noise ratio = 9.55), which is consistent with the color change of the reaction shown in Fig. 4C. Additionally, in order to further investigate the anti-interference ability of the sensing system, secreted proteins MUC1 and EpCAM, along with MCF-7 cell fragments, have been introduced for testing the same detection procedure. As shown in Fig. 4D and Fig. 4E, the signal responses caused by these secreted proteins and cell fragments are almost indistinguishable from the background signal, which is consistent with the colorimetric imaging presented in Fig. 4F. The above experimental results have demonstrated the excellent selectivity of the colorimetric sensing system. Compared to other single-target methods that are prone to cross-reactivity with homologous proteins or non-target exosome subtypes [33–35], our dual-aptamer proximity strategy significantly enhances specificity by requiring simultaneous recognition of two biomarkers (MUC1/EpCAM). This design effectively minimizes interference from single-positive exosomes and protein contaminants.

3.6. Detection of exosomes in serum

To test the stability of the proposed biosensor within complex matrices, target exosomes of varying concentrations were incorporated into 10 % fetal bovine serum (FBS) for comprehensive assay. As evident from Fig. 5, the UV-Vis absorption intensity at 450 nm, steadily increases in direct correlation with the increasing abundance of target exosomes. Crucially, the absorption intensity recorded within the FBS matrix is virtually indistinguishable from that observed in a controlled buffer environment, and the corresponding regression equations derived from both conditions are remarkably congruent, demonstrating the excellent stability and anti-interference ability of our proposed colorimetric analysis method in complex environments.

3.7. Clinical sample analysis

The proposed colorimetric biosensor was ultimately employed to identify exosomes in clinical specimens (serum), with the aim of

assessing its potential for clinical applications. Fig. 6A schematically illustrates the workflow of clinical sample analysis, which involves serum collection from breast cancer patients and healthy individuals, and exosome detection via the amplification cascade. The experiment incorporated samples from 12 Luminal A breast cancer patient individuals (PI) and an equivalent number of healthy individuals (HI), with informed consent secured from all participants. As anticipated, the UV-Vis absorption intensity recorded in serum samples from healthy donors is markedly weaker compared to that in samples from breast cancer patients (Figs. 6B and 6C). Furthermore, the independent sample t-test statistical analysis revealed a statistically significant difference in signal response between the two groups: HI and PI (Fig. 6D). The distinct colorimetric responses are further visualized in Fig. 6E, where reaction solutions from Luminal A breast cancer exhibit a pronounced blue hue compared to the faint color of healthy controls. Clearly, the developed colorimetric biosensor demonstrates exceptional performance in distinguishing MUC1/EpCAM-positive breast cancer patients from healthy individuals, underscoring its promising potential for clinical cancer diagnosis.

4. Conclusion

In conclusion, by leveraging the robust amplification cascade triggered by the proximity effect, utilizing Pt@AuNPs as versatile signal tags, and constructing a multivalent capture interface, we successfully developed a colorimetric biosensor capable of achieving precise and sensitive detection of tumor-derived exosomes. The biosensor achieves a detection limit of 194 particles/ μL with dual-target specificity, outperforming the gold standard method (ELISA) and many existing methods in sensitivity and clinical utility (Table S2 and Table S4). In our design, the dual-molecular recognition mechanism harnessing the proximity effect can substantially elevate the analysis accuracy, enabling the precise identification of specific exosomes amidst various interfering substances, including other tumor-derived exosomes, cell fragments, and secreted proteins. The integration of multiple signal amplification strategies, encompassing 3W-CHA, RCA, nanzyme catalysis, and multivalent capture mechanisms, imparts satisfactory sensitivity to the colorimetric biosensor, enabling the detection of target exosomes at an ultra-low concentration. More significantly, the proposed biosensor demonstrates reliable performance in complex matrices and clinical serum samples, effectively distinguishing MUC1/EpCAM-positive breast cancer patients (e.g., Luminal A subtypes) from healthy donors. Consequently, the developed colorimetric biosensor holds the potential to promote accurate diagnosis and personalized treatment of cancer. Notably, the multivalent capture interface enables parallel processing of multiple samples on a single microplate, which could be readily adapted to automated systems for high-throughput clinical

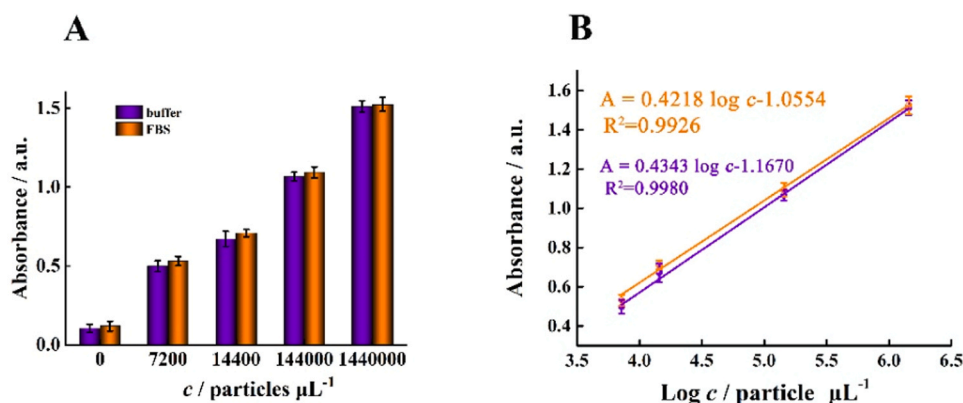


Fig. 5. (A) Signal responses of the proposed colorimetric biosensor toward different abundance exosomes in buffer and 10 % FBS. (B) Correlation curves derived from (A). Error bars: SD, $n = 3$.

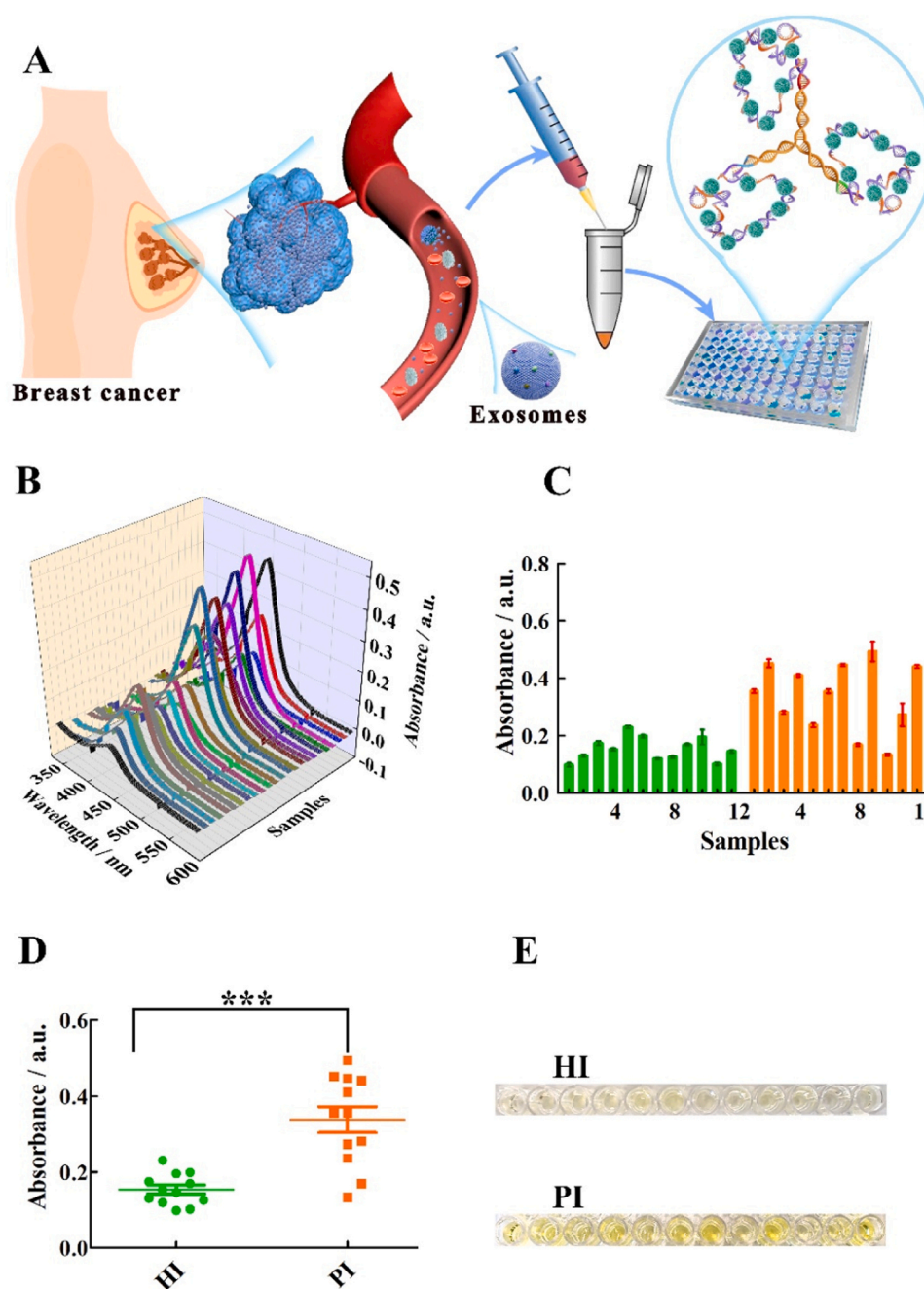


Fig. 6. (A) Principle of clinical sample analysis. (B) The UV-vis absorption spectra obtained from serum samples of 12 healthy individuals and 12 Luminal A breast cancer individuals. (C) Statistical results of the mean UV-Vis absorption peak intensities at 450 nm derived from triplicate measurements of the experiments shown in (B). (D) The statistical results of *t*-test (***, $p < 0.001$). (E) Photographs of the reaction solutions corresponding to the serum samples from healthy individuals and Luminal A breast cancer individuals. Error bars: SD, $n = 3$.

screening. Furthermore, the visual readout eliminates the need for specialized equipment, streamlining workflow in resource-limited settings. Future efforts will focus on enhancing the reaction kinetics and integrating microfluidic architectures to automate fluidic control and reduce manual intervention, thereby enhancing scalability.

CRediT authorship contribution statement

Kou Beibei: Investigation. **Ou Sha:** Investigation. **Hu Zuquan:** Writing – review & editing, Formal analysis. **Wu Shuai:** Writing – review & editing, Formal analysis. **Peng Ying:** Writing – review & editing, Project administration, Formal analysis. **Deng Ying:** Writing – review & editing, Software, Investigation. **Zhao Xiong:** Writing – original draft,

Software, Methodology, Investigation, Conceptualization. **Liu Kaiyuan:** Investigation. **Ren Haohua:** Investigation. **Xiao Jiating:** Data curation.

Declaration of Competing Interest

The authors declare that they have no known competing financial interests or personal relationships that could have appeared to influence the work reported in this paper.

Acknowledgements

Xiong Zhao and Ying Deng contributed equally to this work. This work is supported by the National Natural Science Foundation of China

(82360364); the Natural Science Foundation of Guizhou Province (ZK2024-141); the Science and Technology Fund Project of Guizhou Provincial Health Commission (gzwkj2024-226), the Youth Science and Technology Talents Growth Project of Guizhou Ordinary Colleges and Universities (KY2022-190); Natural Science Foundation Cultivation Project of Guizhou Medical University (22NSFCP32); the High-Level Talent Initiation Project of Guizhou Medical University (J [2023] 003). The Natural Science Foundation of Ningxia (2023AAC05008).

Appendix A. Supporting information

Supplementary data associated with this article can be found in the online version at doi:10.1016/j.snb.2025.137832.

Data availability

Data will be made available on request.

References

- [1] Y. Deng, T. Zhou, K. Hu, Y. Peng, X. Jia, J. Yang, G. Li, An electrochemical biosensor designed with entropy-driven autocatalytic DNA circuits for sensitive detection of ovarian cancer-derived exosomes, *Biosens. Bioelectron.* 250 (2024) 116060.
- [2] S. Wang, L. Zhang, S. Wan, S. Cansiz, C. Cui, Y. Liu, R. Cai, C. Hong, I.T. Teng, M. Shi, Y. Wu, Y. Dong, W. Tan, Aptasensor with expanded nucleotide using DNA nanotetrahedra for electrochemical detection of cancerous exosomes, *ACS Nano* 11 (2017) 3943–3949.
- [3] C. Huang, Y. Zhou, X. Feng, J. Wang, Y. Li, X. Yao, Delivery of engineered primary tumor-derived exosomes effectively suppressed the colorectal cancer chemoresistance and liver metastasis, *ACS Nano* 17 (2023) 10313–10326.
- [4] W. Sun, X. You, X. Zhao, X. Zhang, C. Yang, F. Zhang, J. Yu, K. Yang, J. Wang, F. Xu, Y. Chang, B. Qu, X. Zhao, Y. He, Q. Wang, J. Chen, G. Qing, Precise capture and dynamic release of circulating liver cancer cells with dual-histidine-based cell imprinted hydrogels, *Adv. Mater.* 36 (2024) e2402379.
- [5] K. Whitaker, Earlier diagnosis: the importance of cancer symptoms, *Lancet Oncol.* 21 (2020) 6–8.
- [6] Y.J. Kim, W.Y. Rho, S.M. Park, B.H. Jun, Optical nanomaterial-based detection of biomarkers in liquid biopsy, *J. Hematol. Oncol.* 17 (2024) 10.
- [7] K.A. Preethi, S.C. Selvakumar, K. Ross, S. Jayaraman, D. Tusubira, D. Sekar, Liquid biopsy: exosomal microRNAs as novel diagnostic and prognostic biomarkers in cancer, *Mol. Cancer* 21 (2022) 54.
- [8] R. Uyar, G. Özçelikay-Akyıldız, S.I. Kaya, S. Bereketoğlu Nergis, Ö. Beşbinar, M. A. Ünal, A. Yilmazer, S.A. Özkan, Early cancer detection based on exosome biosensors in biological samples, *Sens. Actuators B* 400 (2024) 134886.
- [9] B. Wei, Y. Xiang, Q. Qin, Y. Xiang, G.J. Zhang, F. Yang, Bioprobes-regulated precision biosensing of exosomes: From the nanovesicle surface to the inside, *Coord. Chem. Rev.* 463 (2022) 214538.
- [10] X.X. Peng, X. Qin, Y. Qin, Y. Xiang, G.J. Zhang, F. Yang, Bioprobes-regulated precision biosensing of exosomes: From the nanovesicle surface to the inside, *Coord. Chem. Rev.* 463 (2022) 214538.
- [11] X. Qin, B. Wei, Y. Xiang, H. Lu, F. Liu, X. Li, F. Yang, Exosome-tuned MOF signal amplifier boosting tumor exosome phenotyping with high-affinity nanostars, *Biosens. Bioelectron.* 245 (2024) 115828.
- [12] X. Qin, Y. Xiang, L. Mao, Y. Yang, B. Wei, H. Lu, X. Li, Y. Zhang, F. Yang, Buoyant metal-organic framework corona-driven fast isolation and ultrasensitive profiling of circulating extracellular vesicles, *ACS Nano* 18 (2024) 14569–14582.
- [13] R. Vogel, F.A. Coumans, R.G. Maltzen, A.N. Boing, K.E. Bonnington, M. L. Broekman, M.F. Broom, E.I. Buzas, G. Christiansen, N. Hajji, S.R. Kristensen, M. J. Kuehn, S.M. Lund, S.L. Maas, R. Nieuwland, X. Osteikoetxea, R. Schnoor, B. J. Scicluna, M. Shambrook, J. de Vrij, S.I. Mann, A.F. Hill, S. Pedersen, A standardized method to determine the concentration of extracellular vesicles using tunable resistive pulse sensing, *J. Extracell. Vesicles* 5 (2016) 31242.
- [14] X. Gao, X. Teng, Y. Dai, J. Li, Rolling circle amplification-assisted flow cytometry approach for simultaneous profiling of exosomal surface proteins, *ACS Sens.* 6 (2021) 3611–3620.
- [15] X. Liu, Z. Zong, M. Xing, X. Liu, J. Li, D. Liu, pH-mediated clustering of exosomes: breaking through the size limit of exosome analysis in conventional flow cytometry, *Nano Lett.* 21 (2021) 8817–8823.
- [16] V. Sharma, F. Nikolajeff, S. Kumar, Employing nanoparticle tracking analysis of salivary neuronal exosomes for early detection of neurodegenerative diseases, *Transl. Neurodegener.* 12 (2023) 7.
- [17] X. Zhang, X. Zhu, Y. Li, X. Hai, S. Bi, A colorimetric and photothermal dual-mode biosensing platform based on nanozyme-functionalized flower-like DNA structures for tumor-derived exosome detection, *Talanta* 258 (2023) 124456.
- [18] R. Huang, L. He, Y. Xia, H. Xu, C. Liu, H. Xie, S. Wang, L. Peng, Y. Liu, Y. Liu, N. He, Z. Li, A sensitive aptasensor based on a hemin/G-Quadruplex-assisted signal amplification strategy for electrochemical detection of gastric cancer exosomes, *Small* 15 (2019) e1900735.
- [19] Y. Wang, H. Jie, H. Ye, Y. Zhang, N. Li, J. Zhuang, Methylene blue-stained single-stranded DNA aptamers as a highly efficient electronic switch for quasi-reagentless exosomes detection: an old dog with new tricks, *Anal. Chem.* 95 (2023) 18166–18173.
- [20] L. Yang, X. Yin, B. An, F. Li, Precise capture and direct quantification of tumor exosomes via a highly efficient dual-aptamer recognition-assisted ratiometric immobilization-free electrochemical strategy, *Anal. Chem.* 93 (2020) 1709–1716.
- [21] H. Xu, C. Liao, P. Zuo, Z. Liu, B.C. Ye, Magnetic-based microfluidic device for on-chip isolation and detection of tumor-derived exosomes, *Anal. Chem.* 90 (2018) 13451–13458.
- [22] Y. Tang, Y. Chen, Y. Liu, Y. Xia, F. Zhao, B. Zeng, Detection of gastric cancer-associated d-amino acids and carcinoembryonic antigen by colorimetric and immuno ECL sensing platform based on the catalysis of N/S-doped carbon dots @ N-rich porous carbon nanoenzyme, *Anal. Chem.* 94 (2022) 17787–17794.
- [23] Z. Gao, H. Ye, D. Tang, J. Tao, S. Habibi, A. Minerick, D. Tang, X. Xia, Platinum-decorated gold nanoparticles with dual functionalities for ultrasensitive colorimetric in vitro diagnostics, *Nano Lett.* 17 (2017) 5572–5579.
- [24] B. Lin, T. Tian, Y. Lu, D. Liu, M. Huang, L. Zhu, Z. Zhu, Y. Song, C. Yang, Tracing tumor-derived exosomal PD-L1 by dual-aptamer activated proximity-induced droplet digital PCR tracing tumor-derived exosomal PD-L1 by dual-aptamer activated proximity-induced droplet digital PCR, *Angew. Chem. Int. Ed.* 60 (2021) 7582–7586.
- [25] X. Yu, W. Lin, Q. Lai, J. Song, Y. Liu, R. Su, Q. Niu, L. Yang, C. Yang, H. Zhang, Z. Zhu, ARMOR: auto-assembled resilient biomimetic calcified ornaments for selective cell protection by dual-aptamer-driven hybridization chain reaction, *Angew. Chem. Int. Ed.* 62 (2023) e202301083.
- [26] X. Li, B. Sun, J. Zhu, M. Qian, Y. Chen, Construction of a mass-tagged oligo probe set for revealing protein ratiometric relationship associated with EGFR-HER2 heterodimerization in living cells, *Anal. Chem.* 94 (2022) 8838–8846.
- [27] F. Schueder, J. Lara-Gutiérrez, D. Haas, K.S. Beckwith, P. Yin, J. Ellenberg, R. Jungmann, Super-resolution spatial proximity detection with proximity-PAIN, *Angew. Chem. Int. Ed.* 60 (2020) 716–720.
- [28] X. Chang, C. Zhang, C. Lv, Y. Sun, M. Zhang, Y. Zhao, L. Yang, D. Han, W. Tan, Construction of a multiple-aptamer-based DNA logic device on live cell membranes via associative toehold activation for accurate cancer cell identification, *J. Am. Chem. Soc.* 141 (2019) 12738–12743.
- [29] X. Liu, Y. Xu, R. Montes, F. Herrera, Social network group decision making: managing self-confidence-based consensus model with the dynamic importance degree of experts and trust-based feedback mechanism, *Inform. Sci.* 505 (2019) 215–232.
- [30] S. Yang, X. Zhan, X. Tang, S. Zhao, L. Yu, M. Gao, D. Luo, Y. Wang, K. Chang, M. Chen, A multiplexed circulating tumor DNA detection platform engineered from 3D-coded interlocked DNA rings, *Bioact. Mater.* 10 (2022) 68–78.
- [31] Z. Qing, G. Luo, S. Xing, Z. Zou, Y. Lei, J. Liu, R. Yang, Pt–S bond-mediated nanoflakes for high-fidelity intracellular applications by avoiding thiol cleavage, *Angew. Chem. Int. Ed.* 59 (2020) 14044–14048.
- [32] B. Liu, J. Liu, Freezing directed construction of bio/nano interfaces: reagentless conjugation, denser spherical nucleic acids, and better nanoflakes, *J. Am. Chem. Soc.* 139 (2017) 9471–9474.
- [33] Y. Zhou, Q. Chen, S. Zhong, H. Liu, K. Koh, H. Chen, Ti₃C₂Tx MXene-facilitated non-selective trapping effect: efficient SERS detection of exosomal PD-L1, *Biosens. Bioelectron.* 237 (2023) 115493.
- [34] S. Wang, L. Zhang, S. Wan, S. Cansiz, C. Cui, Y. Liu, R. Cai, C. Hong, I.T. Teng, M. Shi, Y. Wu, Y. Dong, W. Tan, Aptasensor with expanded nucleotide using DNA nanotetrahedra for electrochemical detection of cancerous exosomes, *ACS Nano* 11 (2017) 3943–3949.
- [35] Y. Wang, H. Jie, H. Ye, Y. Zhang, N. Li, J. Zhuang, Methylene blue-stained single-stranded DNA aptamers as a highly efficient electronic switch for quasi-reagentless exosomes detection: an old dog with new tricks, *Anal. Chem.* 95 (2023) 18166–18173.

Xiong Zhao is a teaching assistant at Guizhou Medical University in China and devotes to nanomaterials and their applications in biosensors.

Ying Deng is a PhD candidate in the School of Life Sciences at Nanjing University in China.

Kaiyuan Liu is a MS candidate at Guizhou Medical University in China.

Jiating Xiao is a MS candidate at Guizhou Medical University in China.

Haohua Ren is a MS candidate at Guizhou Medical University in China.

Sha Ou is an associate professor of Guizhou Medical University in China. Her work is devoted to nanostructured functional materials and their applications in biosensors.

Beibei Kou is an associate professor of Ningxia University in China. Her work is devoted to nanostructured functional materials and their applications in biosensors.

Shuai Wu is a research associate in the First Affiliated Hospital with Nanjing Medical University in China.

Zuquan Hu is a professor of Guizhou Medical University in China. His work is devoted to biosensors, nanostructured functional materials and their applications.

Ying Peng is an associate professor of Guizhou Medical University in China. She received her PhD degree in biology from Nanjing University (China) in 2022. The main research interests of associate professor Peng are chemical sensors and biosensors.